INTERNATIONAL JOURNAL FOR NUMERICAL METHODS IN FLUIDS
Int. J. Numer. Meth. Fluids 2004; **46**:415–433 (DOI: 10.1002/fld.756)

Passive control of the flow around a square cylinder using porous media

Charles-Henri Bruneau*,† and Iraj Mortazavi

Mathématiques Appliquées de Bordeaux, Université Bordeaux 1, 351 cours de la Libération, F-33405 Talence

SUMMARY

The passive control of bluff body flows using porous media is investigated by means of the penalization method. This method is used to create intermediate porous media between solid obstacles and the fluid in order to modify the boundary layer behaviour. The study covers a wide range of two-dimensional flows from low transitional flow to fully established turbulence by direct numerical simulation of incompressible Navier–Stokes equations. A parametric study is performed to illustrate the effect of the porous layer permeability and thickness on the passive control. The numerical results reveal the ability of porous media to both regularize the flow and to reduce the drag forces up to 30%. Copyright © 2004 John Wiley & Sons, Ltd.

KEY WORDS: incompressible bluff body flows; passive control; porous media; penalization method

1. INTRODUCTION

Bluff bodies are found in many engineering applications including heat exchangers, risers in marine technology, road vehicles, aircrafts, buildings and bridges among others. Their wakes can generate large unsteady forces which have the potential to damage the structural integrity of the bluff body itself or to decrease its aerodynamical capabilities. For this reason, many methods have been proposed over the recent years to control the wake vortex dynamics with the aim of weakening the vortex shedding and reducing the amplitude of the fluctuating lift as well as the drag.

An efficient technique to achieve these purposes is the passive control. Passive control is defined here by a flow manipulation using geometrical effects and no extra energy variations. Nominally methods such as compliant walls like the dolphin skeen [1, 2], ribelets [3, 4], splitter plates and base bleed [5], wavy or rough surfaces [6] have been used in the past to weaken vortex shedding and reduce the base drag and the hydrodynamic instabilities [6, 7]. The sur-

*Correspondence to: Charles-Henri Bruneau, Mathématiques Appliquées de Bordeaux, Université Bordeaux 1, 351 cours de la Libération, F-33405 Talence.
†E-mail: bruneau@math.u-bordeaux.fr

Published online 16 August 2004
Copyright © 2004 John Wiley & Sons, Ltd.
Received 21 August 2003
Revised 23 April 2004

face roughness of the bluff body produces a shift of the transition to turbulence towards lower Reynolds number regimes [6]. Some beneficial effects of passive porous, rough or permeable surfaces on boundary layer characteristics have been reported [8–11]. The methodology used in this work consists in separating the solid surface from the flow by a porous interface. The idea is to generate an intermediate flow which reduces the boundary layer effects, specially to decrease the vorticity. This procedure is applied to control vortex flows around a square cylinder.

To simulate the global flow both in the porous and fluid media, it is necessary to solve simultaneously the Darcy equations in the porous medium and the Navier–Stokes equations in the fluid. This is quite difficult to handle as it requires on the one hand to couple two simulations and on the other hand to find out the right condition at the interface of the two media. One way to avoid these difficulties is to use the penalization method where various values of the permeability coefficient will represent the bluff body, the porous medium and the fluid. The penalization method is a fictitious domain method which is very easy to implement, robust and efficient. It has been shown that this method can be used successfully to simulate flows with obstacles and that the use of the permeability term corresponds to solve Darcy equations in the solids [12]. The main advantage of this method is that it needs neither the mesh to fit the boundaries nor to specify no-slip boundary conditions. In addition it allows to compute the pressure as a continuous field on the whole domain including the solids, and the lift and drag coefficients by integrating the penalization term inside the solid bodies [13]. Here, we propose to use the method to modellize the flow in the three different media—solid, fluid and porous medium. In fact each medium can be considered as a porous medium. The fluid is identified to a porous medium of infinite permeability, and the solids are identified to a porous medium of zero permeability. So, a value in between takes place for a porous medium. In this paper, the influence of the porous media permeability on the characteristics of the flow around obstacles is studied. We shall see on a parametric study that there exists a range of optimal values of the permeability coefficient K to influence the vortex dynamics. We shall focus on the delay of transition to turbulence, the amount of enstrophy and the drag and lift forces reduction. Furthermore, we shall show that for a significant range of thicknesses the passive control strategy is efficient even if better results are obtained when the thickness is larger. Once the parametric study fulfilled, the numerical experiments focus on three different flow regimes, low transitional, high transitional and turbulent that correspond to Reynolds numbers 300, 3000 and 30 000, respectively. These numerical tests show that the passive control is always efficient for a good choice of the parameters.

2. MODELLIZATION AND NUMERICAL SIMULATION

2.1. The penalization method

In this work, we want to modellize three media (a solid, a saturated porous medium and an incompressible fluid) with the same equation using the penalization method. The Navier–Stokes equations governing an incompressible newtonian fluid flow in a domain Ω are

$$\rho\partial_t U + \rho(U\cdot\nabla)U - \mu\Delta U + \nabla p = 0 \quad \text{in } \Omega_T = \Omega\times(0,T) \tag{1}$$

$$\operatorname{div} U = 0 \quad \text{in } \Omega_T \tag{2}$$

Copyright © 2004 John Wiley & Sons, Ltd.

where ρ is the density of the fluid, $U=(u,v)$ is the velocity in two dimensions, p is the pressure and μ is the viscosity of the fluid. These equations can be linked to the Forchheiner–Navier–Stokes equations for the porous medium. Indeed, assuming that the fluid saturating the porous medium is Boussinesq, we get Brinkman's equation (that is valid only for high porosities close to one [14]) obtained from Darcy's law for an horizontal flow without gravity by adding the diffusion term

$$\nabla p = -\frac{\mu}{k}\Phi U + \tilde{\mu}\Phi\Delta U \tag{3}$$

then adding the inertial terms with the Dupuit–Forchheiner relationship [14], the Forchheiner–Navier–Stokes equations

$$\rho\partial_t U + \rho(U\cdot\nabla)U + \nabla p = -\frac{\mu}{k}\Phi U + \tilde{\mu}\Phi\Delta U \tag{4}$$

where k is the intrinsic permeability, $\tilde{\mu}$ is Brinkman's effective viscosity and Φ is the porosity. As Φ is close to 1 we can approximate $\tilde{\mu}\approx\mu/\Phi$ [15] and get the equation

$$\rho\partial_t U + \rho(U\cdot\nabla)U + \nabla p = -\frac{\mu}{k}\Phi U + \mu\Delta U \tag{5}$$

Then a non-dimensionalization using the usual substitutions including the mean velocity of the fluid $\bar{U}$ and the height of the domain H

$$U = U'\bar{U};\quad x = x'H;\quad t = t'\frac{H}{\bar{U}} \tag{6}$$

yields the penalized adimensional Navier–Stokes equations or Brinkman–Navier–Stokes equations written as

$$\partial_t U' + (U'\cdot\nabla)U' - \frac{1}{Re}\Delta U' + \frac{U'}{K} + \nabla p' = 0 \quad \text{in } \tilde{\Omega}_T = \tilde{\Omega}\times(0,T) \tag{7}$$

$$\operatorname{div} U' = 0 \quad \text{in } D_T \tag{8}$$

where $K=\rho k\Phi\bar{U}/\mu H$ is the adimensional coefficient of permeability of the medium, $Re=\rho\bar{U}H/\mu$ is the Reynolds number based on the height of the domain and $\tilde{\Omega}$ is the full domain including the porous and solid media ($\tilde{\Omega}=\Omega\cup\Gamma_0\cup\Omega_0$). Indeed, in the fluid the permeability coefficient goes to infinity, the penalization term vanishes and we recover the adimensional Navier–Stokes equations. In the solid the permeability coefficient goes to zero and it has been shown in Reference [12] that solving these equations corresponds to solve Darcy's law in the solid and that the velocity is proportional to K. The main advantage of this method is that it needs neither the mesh to fit the boundaries nor to specify no-slip boundary conditions. In addition it allows to compute the pressure as a continuous field on the whole domain including the solids, and the lift and drag coefficients by integrating the penalization term inside the solid bodies [13]. These equations simplify considerably the domain exchange (solid to fluid, solid to porous medium or fluid to porous medium) as the same equation is solved in the whole domain. The only thing to do is to define the permeability coefficient K on each velocity grid point. Numerically, the fluid is considered as a porous medium with a very high permeability ($K=10^{16}$) and the bodies are considered as porous media with a

Copyright © 2004 John Wiley & Sons, Ltd.

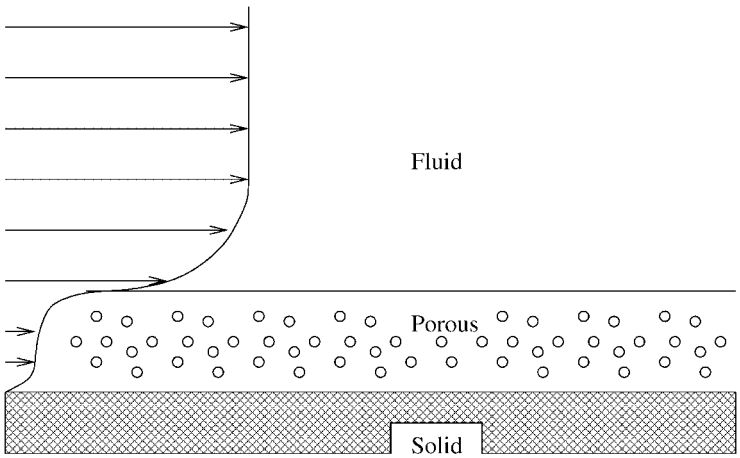

Figure 1. Example of velocity profile in the vicinity of the porous layer.

very small permeability ($K = 10^{-8}$). It was shown by different approaches that solving the Equations (7), (8) is equivalent to solve the Navier–Stokes equations in the fluid with a Fourier-like boundary condition instead of the no-slip boundary condition (see in particular References [16, 17]). This is exactly the effect of the addition of a porous layer as stated in Reference [14] and illustrated in Figure 1. In this work, this property is explored to reduce the shear effects in the boundary layer and control the flow. Let us point out to the reader that for water we get $K = 10^6 k\Phi\tilde{U}/H$. So setting $K = 10^{-8}$ in the bodies corresponds to a very condensed medium that behaves like a solid medium for the simulation times of the fluid flow [12, 13]. In addition, an intermediate value as $K = 10^{-1}$ corresponds to a very permeable porous medium like clean gravel [14].

From now to the end of the paper the variables (U', p') of Equations (7), (8) are denoted (U, p). To validate the penalization method, an easy numerical test is presented for the flow behind a small square bluff body with a size $D = 0.2$ inside a channel of height $H = 1$. The computational domain $\tilde{\Omega} = (0, 4) \times (0, 1)$ corresponds to a portion of the channel and the centre of the square is located at the position $(1.1, 0.5)$. The Reynolds number based on the size of the obstacle is equal to $Re_D = Re \times D$. The penalization method is compared to the standard Dirichlet no-slip boundary condition $U = 0$ for the flow obtained at $Re_D = 80$ behind a square obstacle. The computation is performed on a uniform 320×80 cells mesh so that the mesh fits the square obstacle. The pressure field which is continuous for the penalization method is represented in Figure 2. This pressure field continuity on the whole domain and the possibility of computing the drag and the lift forces by the integration of the penalization term inside the solid bodies are two beneficial characteristics of the penalization method [13]. We have checked that a direct computation of these forces gives the same values. As shown in the figure, the solutions are very close to each other outside the obstacle. Therefore, on this test case, it is shown that the penalization method generates the same flow that the no-slip boundary condition. More details about the penalization method and its convergence can be found in Reference [12]. Furthermore, a porous medium is modellized choosing an appropriate value of the penalization parameter K between the fluid and solid values. The range of permeability

Copyright © 2004 John Wiley & Sons, Ltd.

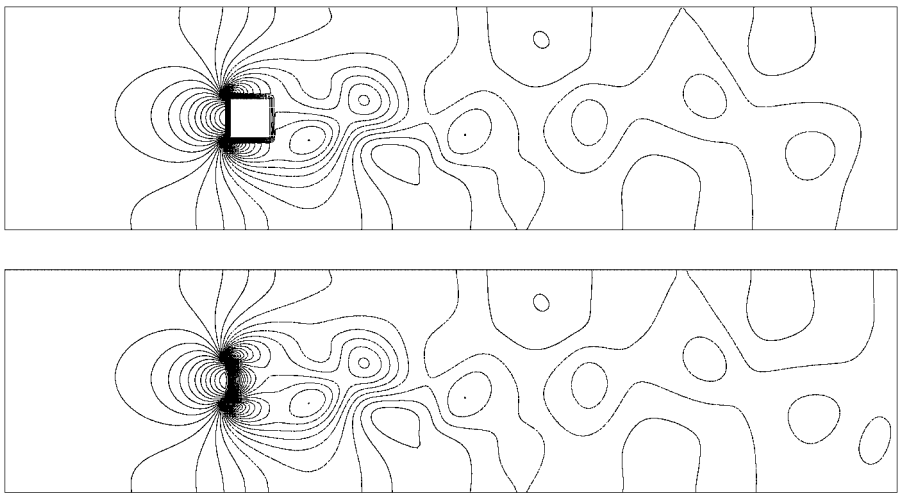

Figure 2. Comparison of the solutions (pressure field) computed with Dirichlet boundary condition and the penalization method with $K = 10^{-8}$ at Reynolds number $Re_D = 80$.

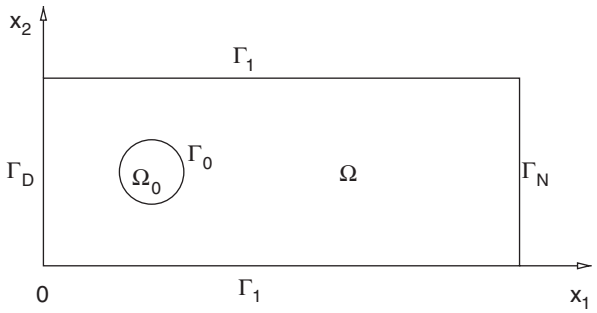

Figure 3. Computational domain.

coefficient values varies from $K = 10^{-3}$ to 100. Lower values correspond to porous media too close to the solid behaviour to control efficiently the flow. On the opposite, upper values are almost dominated by the flow and thus are equivalent to reduce the size of the obstacle.

2.2. Initial and boundary conditions

In this paper, we study the flow around obstacles in a portion of a 2D channel or in a 2D free domain. Figure 3 shows the computational domain Ω in the first case with boundaries $\partial\Omega = \Gamma_D \cup \Gamma_0 \cup \Gamma_1 \cup \Gamma_N$. Equations (7), (8) are coupled to an initial condition

$$U(x,0) = U_0(x) \quad \text{in } \Omega \tag{9}$$

where U_0 is the initial flow imposed on Ω. On the entrance section Γ_D, the far field flow condition U_∞ with a Poiseuille profile is applied. On the solid walls Γ_1 the no-slip boundary

Copyright © 2004 John Wiley & Sons, Ltd.

condition $U=0$ is imposed. On the boundaries of the obstacles Γ_0 the no-slip condition is achieved by the penalization method.

On the artificial outlet section Γ_N, a non-reflecting boundary condition is used to convey properly the shear effects [18]:

$$\sigma(U,p)n+\tfrac{1}{2}(U\cdot n)^{-}(U-U_{\text{ref}})=\sigma(U_{\text{ref}},p_{\text{ref}})n \tag{10}$$

where σ is the stress tensor, n is the unit normal vector pointing outside of the domain, $(U_{\text{ref}}, p_{\text{ref}})$ is a reference flow and with the notation $a=a^{+}-a^{-}$. In (10), the non-linear term is zero when the flow leaves the domain and so the condition reduces to fix the traction equal to the traction of the reference flow. The reference flow is chosen equal to a Poiseuille profile with zero pressure for laminar flows and to the computed flow at the exit section for transitional or turbulent flows, which is the case in this paper. In this latest case strong eddy structures cross the artificial boundary and the non-linear term is active to avoid reflecting waves. Another advantage of this boundary condition is that no buffer zone is needed and that the computational domain corresponds to the real domain of investigation. The same boundary condition is used to compute the flow around a bluff body in an open domain. In that case the artificial boundary condition is specified everywhere except on the entrance section. In both cases the flow is computed in a small box without creating any reflections.

2.3. *The numerical approximation*

The evolution equations are discretized in time by a first-order Euler scheme or a second order Gear scheme with an implicit treatment of the linear terms and an explicit treatment of convection term. The primitive unknowns velocity–pressure are set on staggered grids as illustrated in Figure 4. The spatial approximation is performed using second-order centred finite differences for the linear terms and a third-order upwind Murman scheme for the convection term [19]. The location of the unknowns enforce the divergence-free equation which is discretized on the pressure points. The equations are solved by a strongly coupled method, that means the discretized equations in velocity and pressure are solved simultaneously. The whole problem is solved using a multigrid method and on each grid the solution is obtained by means of a cell by cell Gauss–Seidel iterative procedure. For instance, the set of grids varies from the coarsest 20×5 uniform grid to the finest 640×160 or 1280×320 uniform

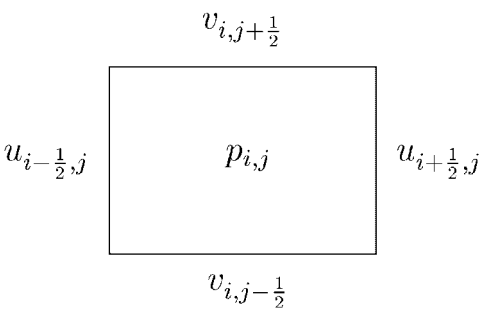

Figure 4. A staggered cell.

Copyright © 2004 John Wiley & Sons, Ltd.

grid depending on the needed accuracy. The choice of uniform grids is necessary to maintain the accuracy of the finite differences schemes.

3. PASSIVE FLOW CONTROL

3.1. Parametric study

It's well known that when a viscous fluid flows past a bluff body, owing to the adverse pressure gradient, a boundary layer separation occurs. The result of flow separation is a high loss of energy in the fluid and the disruption of an approximate potential flow pattern and of the corresponding pressure distribution. In practice, separation decreases the performance of any fluid handling device. One of the reasons is linked to the formation of vortices. To a body immersed in a flowing fluid, vortices are undesirable on three major accounts, oscillations induced by the non-symmetric and unsteady shedding of vortices, high pressure drag and wake buffeting of leeward structures. As mentioned before, to reduce boundary layer effects, a passive control method using porous surfaces is introduced [20].

The penalization method offers the capability to introduce easily intermediate porous regions between the obstacles and the fluid. It is a way to implement passive control strategies to influence the transition to turbulence, to manipulate vortical structures behaviour and interactions or to contribute to drag reduction. The parametric study is performed in a confined domain around an obstacle in order to better represent global quantities like the enstrophy which are more exact in a closed domain. Here, the passive control is done using two porous layers located inside the upper and lower parts of a square obstacle. Two main questions arise: What is the influence of the value of the permeability K and what is the influence of the thickness of the porous layers on the flow behaviour? We first present a parametric study for the flow behind this small square bluff body with a size $D = 0.2$, and the centre located at the position $(1.1, 0.5)$ in a no-slip channel of height $H = 1$ and length $L = 4$. We compare the flow behaviour at $Re_D = 300$ for which there is a periodic unsteady solution for different values of K. In this paper we refer to the solid case when the porous layer has the same permeability coefficient as the solid ($K = 10^{-8}$), we refer to the fluid case when the porous layer has the same permeability coefficient as the fluid ($K = 10^{16}$) which corresponds to reduce the height of the obstacle and we refer to the porous case when the porous layer takes a value of the permeability coefficient in between.

To illustrate the efficiency of the control strategy, we propose to plot global quantities as the enstrophy that represents the number and the energy of the vortices. Two other interesting quantities are the drag coefficient and the lift coefficient that correspond to the horizontal and vertical components of the external forces on the body. In this application, the lift force is oscillating around zero. Therefore it is more appropriate to compute the root mean square of the lift coefficient ($\mathrm{CL}_{\mathrm{rms}}$) which measures the permanence and the symmetry of the flow evolution around the bluff body. The results presented in Figures 5 and 6 for a thickness h such that $h/D = 10\%$ show clearly that the total enstrophy and the root mean-square of the lift coefficient defined by

$$Z = \frac{1}{2}\int_{\Omega} |\omega|^2 \, \mathrm{d}x; \quad \mathrm{CL}_{\mathrm{rms}} = \sqrt{\frac{1}{T}\int_0^T CL \, \mathrm{d}t}$$

Copyright © 2004 John Wiley & Sons, Ltd.

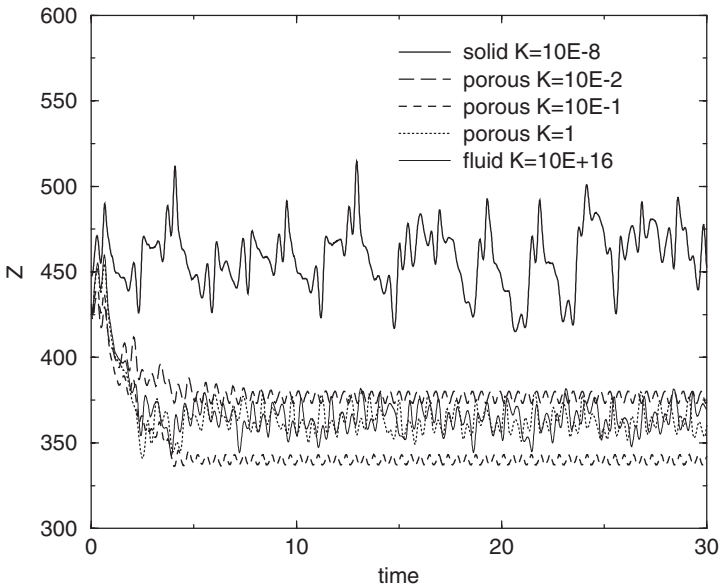

Figure 5. Effect of various permeabilities on the enstrophy evolution for $Re_D = 300$ and $h/D = 10\%$ in a channel with $D/H = 20\%$.

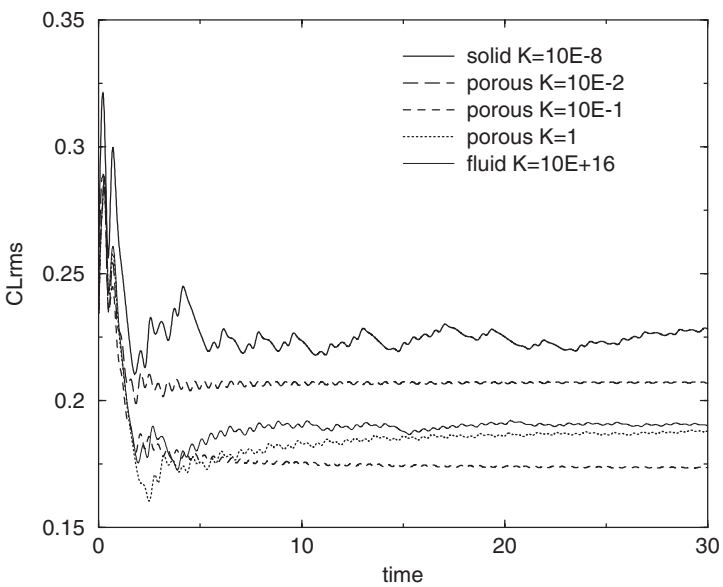

Figure 6. Effect of various permeabilities on the root mean-square of the lift coefficient evolution for $Re_D = 300$ and $h/D = 10\%$ in a channel with $D/H = 20\%$.

Copyright © 2004 John Wiley & Sons, Ltd.

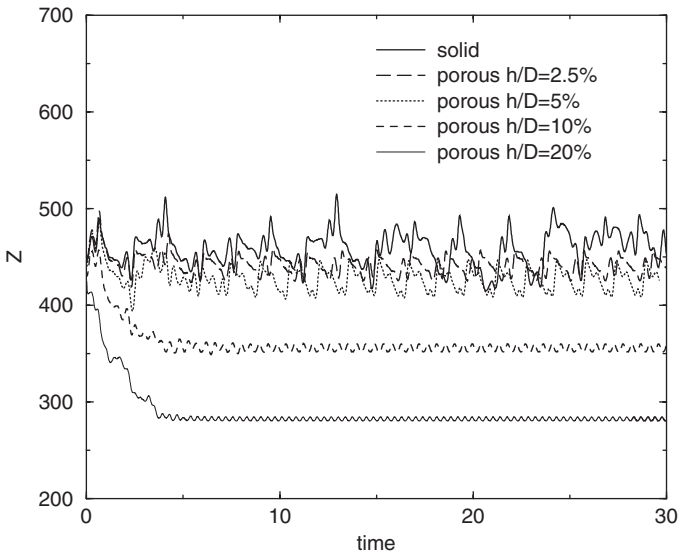

Figure 7. Effect of various porous layer thicknesses on the enstrophy evolution for $Re_D = 300$ and $K = 10^{-1}$ in a channel with $D/H = 20\%$.

are drastically decreased using this passive control strategy. Let us point out to the reader that in both cases the optimal value is reached for $K = 10^{-1}$. Indeed, even if there is an improvement, the values obtained for $K = 10^{-2}$ and 1 are less good. Moreover the optimal values are 5–10% lower than the values obtained for the fluid case although the fluid case corresponds to an obstacle size reduction by 20%. These paradoxal results are due to the fact that the porous medium changes the boundary layer shear properties. The numerical simulations on the finest 640×160 uniform grid and on the finest 1280×320 uniform grid give the same results. Therefore we have reached the grid convergence.

After the permeability coefficient we devote the parametric study to the porous layer thickness h for a given value $K = 10^{-1}$. In order to have enough grid points for thin porous layers, these numerical tests are performed only on the finest 1280×320 grid. We see in Figure 7 that the reduction of the enstrophy occurs whatever the thickness is but becomes more significant for quite large thicknesses. However, we observe in Figure 8 that a wide range of thicknesses give a significant decrease of the CL_{rms} with even lower values than for the fluid case. Moreover for a thicker layer ($h/D = 20\%$) there is a tremendous decrease of the CL_{rms} but this case is not realistic for an industrial application. Both figures illustrate the regularizing effects of this passive control technique.

According to the results of this section, all numerical tests from now until the end of the paper will be performed taking $h/D = 10\%$ and mainly $K = 10^{-1}$.

3.2. *Numerical results*

Many real problems concern the open flow around obstacles (ground vehicles, aircrafts, ships, oil pipe risers, …) at various flow conditions. So it is interesting to explore the capability of the proposed passive control strategy for a wide range of Reynolds numbers applied

Copyright © 2004 John Wiley & Sons, Ltd.

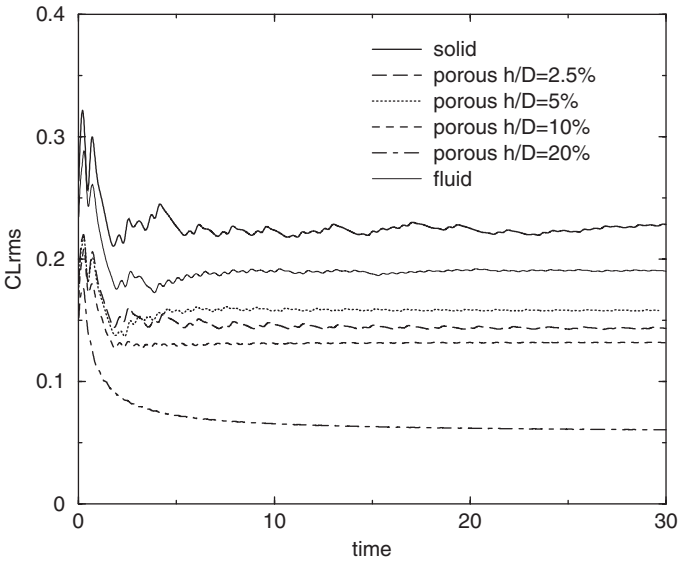

Figure 8. Effect of various porous layer thicknesses on the root mean-square of the lift coefficient evolution for $Re_D = 300$ and $K = 10^{-1}$ in a channel with $D/H = 20\%$.

to such configurations. In this section we consider the flow behind a small square bluff body with a size $D = 0.2$, located at the position $(1.1, 1)$ in an open computational domain $\tilde{\Omega} = (0,5) \times (0,2)$. The real Reynolds number is equal to $Re_D = Re \times D$. Again, the passive control is achieved using two porous layers of height $h = 0.02$ located on the upper and lower sides of the square. We discuss the effects of the passive control for three real Reynolds numbers $Re_D = 300, 3000$ and $30\,000$. The first Reynolds number corresponds to the beginning of the transition where the flow irregularities can be drastically decreased using an appropriate control technique. On the other hand, $Re_D = 3000$ is a more transitional flow with high irregularities, strong eddy shedding and vortex merging and mixing in the flow. The third value correspond to fully developed 2D turbulence. Therefore, the application of porous control procedure to these three flow regimes gives a complementary analysis on the efficiency of the method to control the external bluff body flows. To reach a sufficient accuracy, the set of grid used in the computation varies from the coarsest 25×10 grid to the finest 800×320 grid for $Re_D = 300$ and 3000 and to the finest 1600×640 grid for $Re_D = 30\,000$.

To study the control effects on the flow we analyse the instantaneous vorticity and pressure fields, the evolution of the velocity at a monitoring point and global quantities such as the enstrophy (Z), the drag coefficient (Cd) and the root mean square of the lift coefficient ($\mathrm{CL_{rms}}$). We compare the solid case to the porous case with K varying from $K = 0.1$ to 100 and to the fluid case. As we shall see, larger values of K are needed to control the drag at high Reynolds numbers.

3.2.1. Results at $Re_D = 300$. The first value $Re_D = 300$ has been chosen in order to point out the regularization effects of the passive control by the porous layers which permeability K is chosen equal to 0.1 according to the previous parametric study. Indeed, this Reynolds number

Copyright © 2004 John Wiley & Sons, Ltd.

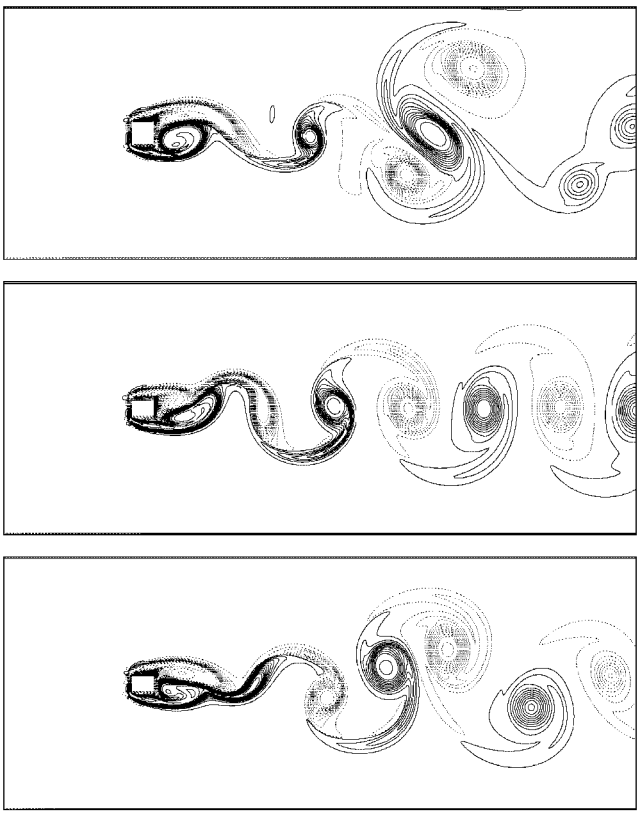

Figure 9. Vorticity field for solid (top), porous with $K = 0.1$ (middle) and fluid (bottom) layers at the same time for $Re_D = 300$ in an open domain. Tabulated isovalues $-40, -30, -20, -15, -12, -10, -9, -8, -7, -6, -5, -4, -3, -2, -1, -0.1, 0.1, 1, 2, 3, 4, 5, 6, 7, 8, 9, 10, 12, 15, 20, 30, 40$.

corresponds to the beginning of the transition. So it is easier to see the flow brought back to a periodic regime. The plots of the vorticity fields in Figure 9 show that the porous interfaces inhibit the vortices interaction in such a way that a regular Karman alley is recovered. The flow obtained is even more regular than for the fluid case. This is also illustrated by the horizontal velocity evolution at a monitoring point downstream the obstacle. Indeed, a periodic signal is obtained only in the porous case (Figure 10). These qualitative observations show the beneficial effects of the porous layer in particular to regularize the flow.

Let us quantify now the control gain by investigating the global quantities. To measure quantitatively the vorticity evolution in the computational domain, the enstrophy history is plotted in Figure 11. It appears clearly that the porous layer is very efficient as the enstrophy production is almost constant along the time and lower than in the two other cases. In the solid case the formation of large tripole structures induce strong peaks of enstrophy whereas in the porous case the vortices are convected in the Karman street without any interaction. Figures 12 and 13 show that an important reduction of the drag coefficient and the CL_{rms} is obtained in the porous case. The drag coefficient history is much more regular than both

Copyright © 2004 John Wiley & Sons, Ltd.

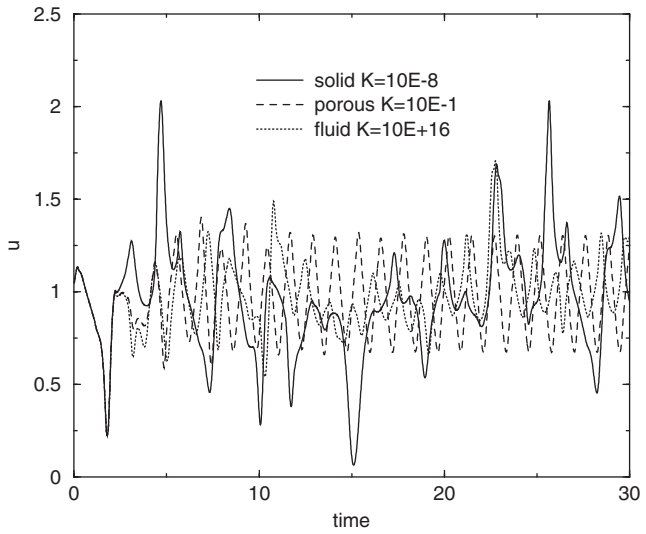

Figure 10. Horizontal velocity history at monitoring point $(4.0625, 0.75)$ for $Re_D = 300$ in an open domain.

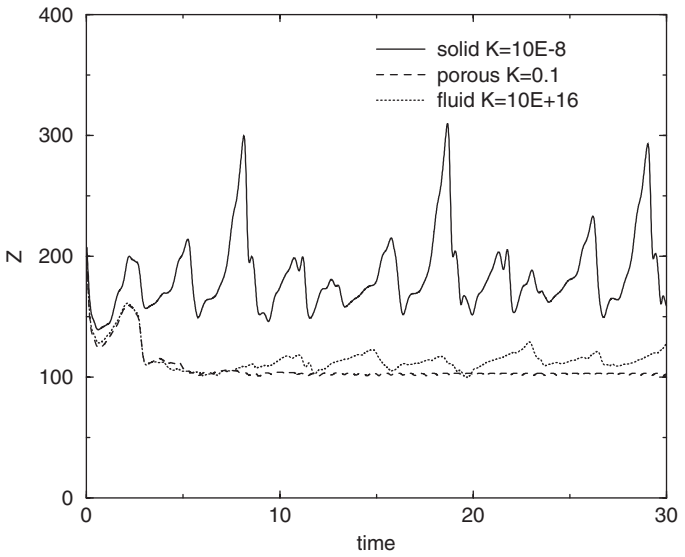

Figure 11. Enstrophy comparison for solid, porous and fluid layers for $Re_D = 300$ and $h/D = 10\%$ in an open domain.

other cases but the fluid case that corresponds to a smaller obstacle yields a slightly better reduction. The root mean square of the lift coefficient evolution is almost constant and its reduction is drastic, even better than in the fluid case. That confirms the observations on the vorticity fields that show a regular vortex shedding process in the porous case. Table I

Copyright © 2004 John Wiley & Sons, Ltd.

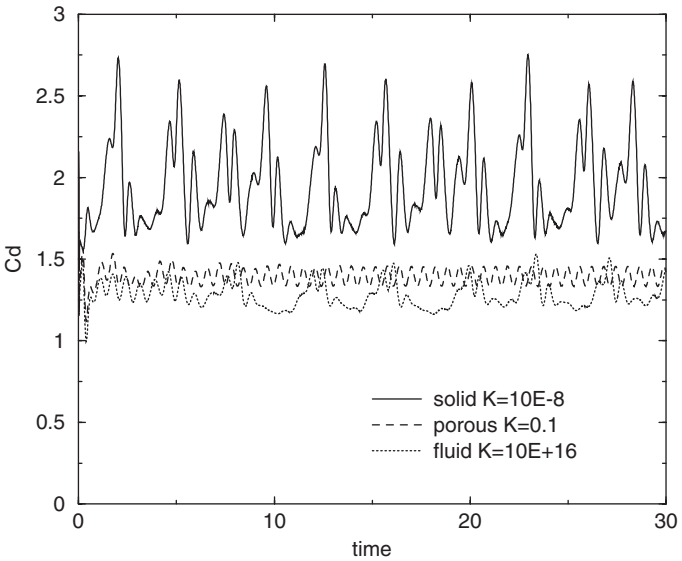

Figure 12. Drag coefficient comparison for solid, porous and fluid layers for $Re_D = 300$ and $h/D = 10\%$ in an open domain.

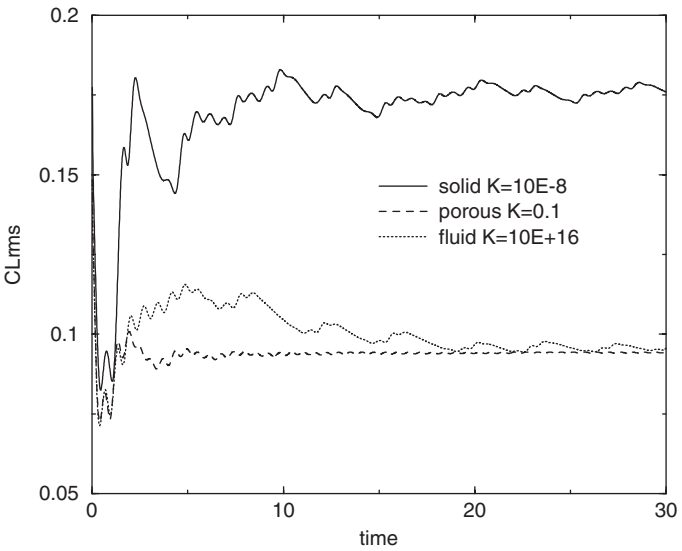

Figure 13. Root mean-square of the lift coefficient evolution for solid, porous and fluid layers for $Re_D = 300$ and $h/D = 10\%$ in an open domain.

contains the mean values of the global quantities and the observed gain compared to the solid case. In the porous case, the reductions are not directly linked to the thickness of the porous layer but to the change of boundary condition from no-slip to Fourier-like (see References [16, 17, 21]).

Copyright © 2004 John Wiley & Sons, Ltd.

Table I. Mean values for $Re_D = 300$.

K	Enstrophy	Drag	CL_{rms}
10^{-8} (solid)	183	1.95	0.176
0.1 (porous)	107 (−42%)	1.39 (−29%)	0.094 (−47%)
10^{16} (fluid)	115 (−37%)	1.28 (−34%)	0.096 (−45%)

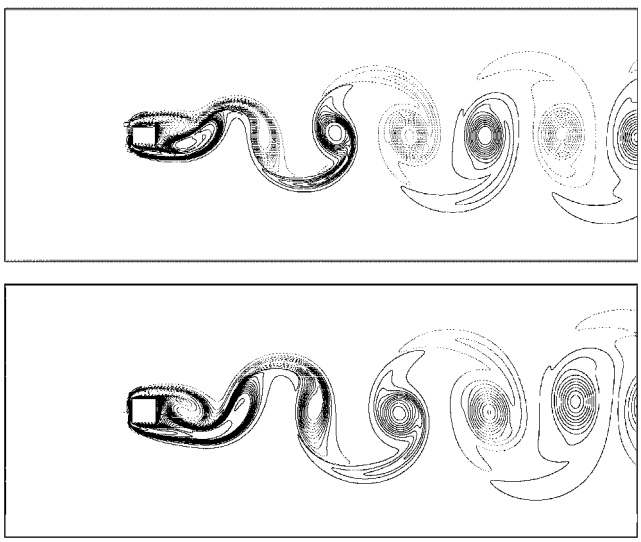

Figure 14. Vorticity field for the porous case with $K = 0.1$ at $Re_D = 300$ (top) and the solid case at $Re_D = 200$ (bottom) in an open domain. Tabulated isovalues $-40, -30, -20, -15, -12, -10, -9, -8, -7, -6, -5, -4, -3, -2, -1, -0.1, 0.1, 1, 2, 3, 4, 5, 6, 7, 8, 9, 10, 12, 15, 20, 30, 40$.

In addition, we observe that the regularization effects are similar to a reduction of the Reynolds number. To confirm that assertion we compare in Figure 14 the flow of the porous case at $Re_D = 300$ to the flow of the solid case at $Re_D = 200$. We see clearly the similarity of the vortex shedding with a Karman street in both cases even if the size of the vortices is different as it is directly linked to the size of the body and the Reynolds number. Finally, the phase portrait of the four cases is plotted in Figure 15 to emphasize the observations above. The vertical component of the velocity with respect to the horizontal component is represented at a monitoring point in the far wake. It is obvious that a fully periodic regime is achieved by the porous case which is even more regular than the $Re_D = 200$ flow whereas the two uncontrolled cases at $Re_D = 300$ exhibit a transistory behaviour.

3.2.2. Results at $Re_D = 3000$. This Reynolds number corresponds to a highly transitional flow generating complex and strong vortex interactions. In the solid case we observe in Figure 16 complex multipole eddy structures whereas the flow is mainly composed of monopole and dipole structures in the porous case with $K = 0.1$. In average, the number of vortices is

Copyright © 2004 John Wiley & Sons, Ltd.

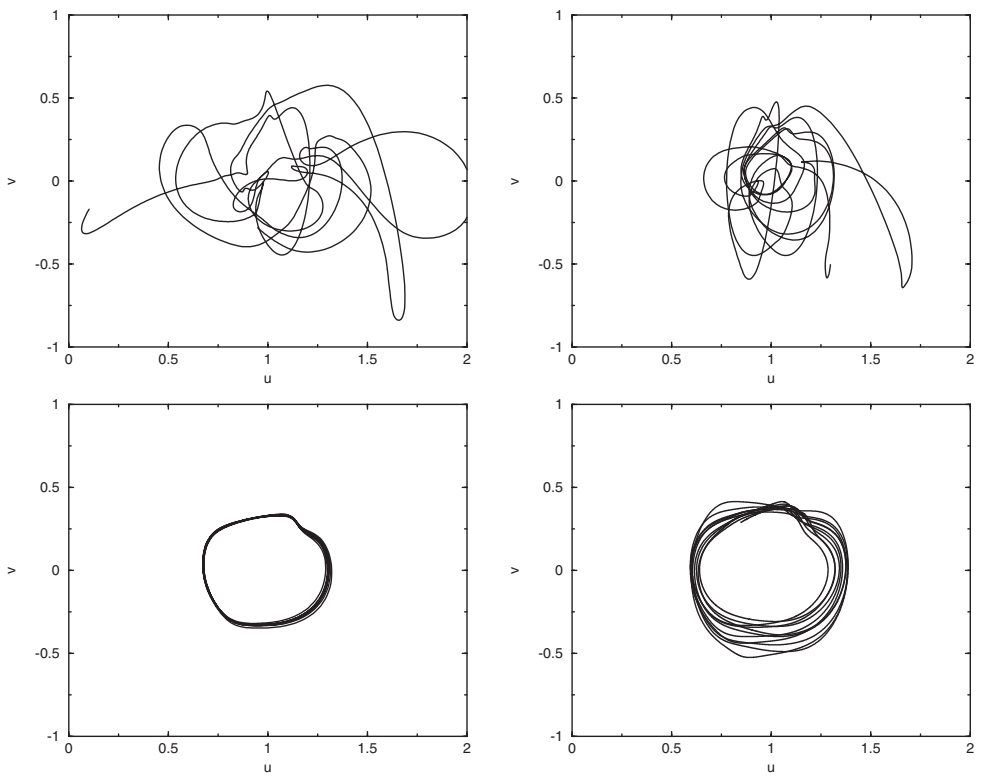

Figure 15. Comparison of phase portraits at monitoring point $(4.0625, 0.75)$ for $Re_D = 300$ and $K = 10^{-8}$ (top left), $K = 10^{16}$ (top right), $K = 0.1$ (bottom left) and for $Re_D = 200$ and $K = 10^{-8}$ (bottom right) in an open domain.

about 30% lower for this latter flow. The pressure fields represented in Figure 17 show that the flow is regularized with much lower pressure gradients as the pressure isolines are less concentrated, in particular around the body. So, introducing the porous layer, both the shear stress and the pressure gradient are weaker and the generated vortices are less energetic. Consequently the convected vortices in the field are more diffused and have less interactions. All these observations confirm the regularization effect of the porous layer even if in this case we do not recover a periodic flow like in the previous numerical test. Table II contains the mean values of the global quantities and the observed gain is 31% for Z, 13% for C_d and 31% for $\mathrm{CL}_{\mathrm{rms}}$ in the porous case with $K = 10^{-1}$ versus 18%, 25% and 18% in the fluid case. The decrease of the enstrophy and the $\mathrm{CL}_{\mathrm{rms}}$ is still very good as the flow is significantly regularized and the transition is delayed by the porous interface. A reduction of 13% for the drag coefficient is already a substantial gain but it can be improved changing the coefficient K, in other words the permeability of the porous medium. For instance it is seen in Table II that with $K = 1$ a drag reduction of 26% is achieved together with a less significant reduction of the two other quantities. This set of results show that the permeability of the porous medium has to be chosen according to the goal of the control. One must know if he wants to give the

Copyright © 2004 John Wiley & Sons, Ltd.

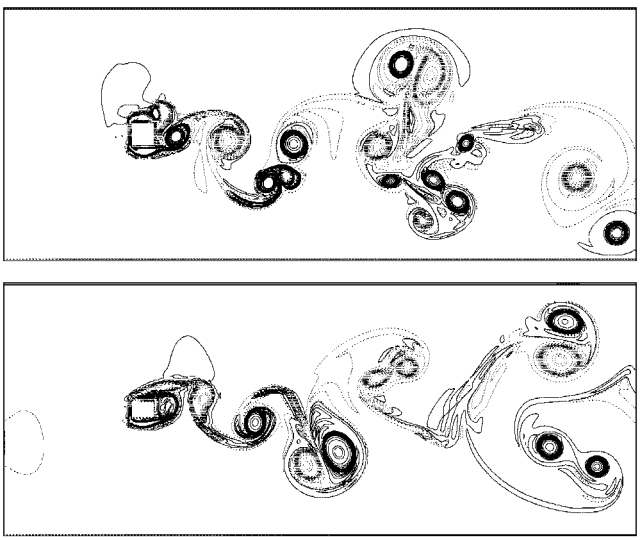

Figure 16. Vorticity field for solid (top) and porous with $K = 0.1$ (bottom) layers at the same time for $Re_D = 3000$ and $h/D = 10\%$ in an open domain. Tabulated isovalues $-40, -30, -20, -15, -12, -10, -9, -8, -7, -6, -5, -4, -3, -2, -1, -0.1, 0.1, 1, 2, 3, 4, 5, 6, 7, 8, 9, 10, 12, 15, 20, 30, 40$.

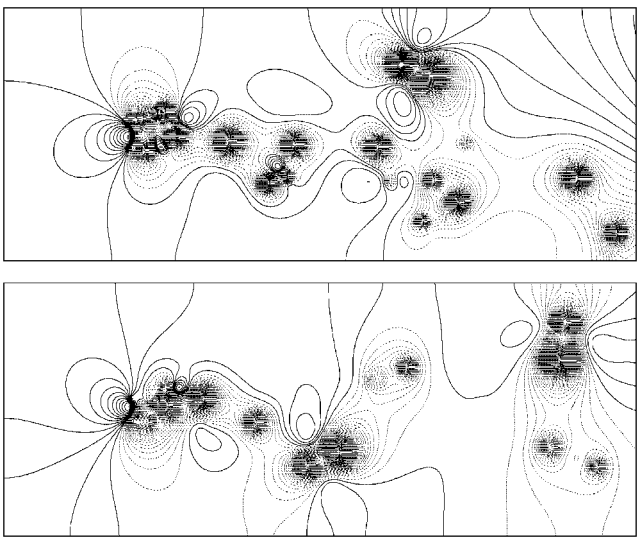

Figure 17. Pressure field for solid (top) and porous with $K = 0.1$ (bottom) layers at the same time for $Re_D = 3000$ and $h/D = 10\%$ in an open domain. Equidistant isovalues from -5 to 5 by step of 0.05.

priority to the flow regularization or to the drag reduction. In conclusion to this subsection, we observe that, for this kind of transitional flows, there is a wide range of values of the permeability at least from $K = 0.1$ to 10 that give a sharp reduction of the global quantities. The higher this coefficient is the closer the solution is to the solution of the fluid case.

Copyright © 2004 John Wiley & Sons, Ltd.

Table II. Mean values for $Re_D = 3000$.

K	Enstrophy	Drag	CL_{rms}
10^{-8} (solid)	597	2.52	0.321
0.1 (porous)	410 (−31%)	2.20 (−13%)	0.221 (−31%)
1 (porous)	457 (−23%)	1.87 (−26%)	0.264 (−18%)
10 (porous)	468 (−22%)	1.89 (−25%)	0.274 (−15%)
10^{16} (fluid)	487 (−18%)	1.90 (−25%)	0.263 (−18%)

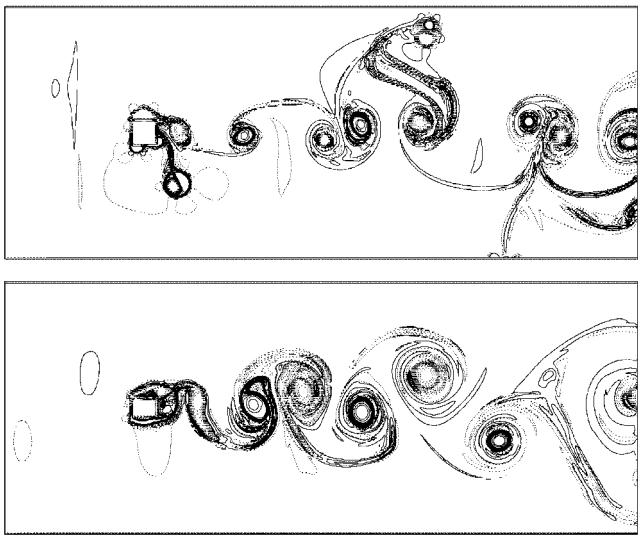

Figure 18. Vorticity field for solid (top) and porous with $K = 0.1$ (bottom) layers at time $t = 30$ for $Re_D = 30\,000$ and $h/D = 10\%$ in an open domain. Tabulated isovalues $-40, -30, -20, -15, -12, -10, -9, -8, -7, -6, -5, -4, -3, -2, -1, -0.1, 0.1, 1, 2, 3, 4, 5, 6, 7, 8, 9, 10, 12, 15, 20, 30, 40$.

3.2.3. Results at $Re_D = 30\,000$. This numerical test corresponds to a fully developed two-dimensional turbulence with chaotic vortex interactions and thin vorticity filaments [22, 23] as shown on top of Figure 18. We start the control with a porous layer of permeability $K = 0.1$. The figure shows that the number of vortical structures decreases and their size increases using the porous layer. This is related to an evolution of complex multipole structures in the solid case towards more simplified vortices in the porous case. The vortex interactions are also simplified to yield almost a Karman street behind the obstacle at time $t = 30$. It seems that diffusive effects are more present in the porous case as the vortices are larger. All these observations show the regularizing effect of the porous layer. This property is also confirmed by the strong decrease of the enstrophy and the CL_{rms} as seen in Table III. However there is a very big increase of the drag coefficient. It shows again that flow regularization and drag reduction are not correlated to each other. Then, according to the results of the previous subsection, we decide to increase the permeability coefficient in order to get better drag

Copyright © 2004 John Wiley & Sons, Ltd.

Table III. Mean values for $Re_D = 30\,000$.

K	Enstrophy	Drag	CL_{rms}
10^{-8} (solid)	1236	2.47	0.430
0.1 (porous)	821 (−34%)	4.54 (+83%)	0.344 (−20%)
1 (porous)	1084 (−12%)	3.70 (+49%)	0.532 (+24%)
10 (porous)	1114 (−10%)	2.11 (−15%)	0.344 (−20%)
100 (porous)	1040 (−16%)	1.61 (−35%)	0.375 (−13%)
10^{16} (fluid)	1012 (−18%)	1.58 (−36%)	0.375 (−13%)

properties. The results for $K = 1, 10$ and 100 confirm our expectations as the drag coefficient decreases smoothly to a gain of 35% which is close to the gain obtained for the fluid case. Indeed, a porous layer of permeability coefficient $K = 100$ seems to be very similar to fluid and could be a limit of porous permeability for our modelling. All the results for the global quantities are gathered in Table III. We observe that the enstrophy and the CL_{rms} are always decreased except for $K = 1$ that gives a surprising 24% increase of the CL_{rms} that could be due to vortex induced vibrations.

4. CONCLUSIONS

The penalization method is used successfully to introduce a new passive control strategy, which consists of implementing a porous layer between the bluff body and the fluid, in order to change the boundary layer characteristics. The porous medium permeability is directly related to the parameter K of the penalization term added to the Navier–Stokes equations. The parametric study shows on the one hand that a wide range of the permeability coefficients K yield a significant control of the flow and on the other hand that a sufficient thickness is needed to achieve a good control. The numerical tests around a square obstacle in an open domain for three Reynolds numbers $Re_D = 300, 3000$ and 30 000 corresponding to three different flow regimes bring several fruitful informations on the capability of the present passive control procedure. The $Re_D = 300$ flow is very interesting because it corresponds to the beginning of the transition. Implementing the porous layer the flow is brought back from a transitional flow to a laminar one. In addition the drag and the CL_{rms} coefficients are drastically reduced. For higher Reynolds numbers corresponding to more complex flows the results are still impressive for a good choice of the permeability coefficient. Nevertheless, the regularization of the flow and the reduction of the drag coefficient are not always obtained simultaneously.

The present passive control method is efficient, cheap and easy to implement and allows to get significant bluff body flows improvement up to a 40% reduction of the global quantities. Some extensions to industrial applications like ground vehicles or riser pipes should be promising.

ACKNOWLEDGEMENTS

The authors thank warmly their colleague Didier Lasseux from mechanics department for the fruitful discussions they had on porous media modellization.

Copyright © 2004 John Wiley & Sons, Ltd.

REFERENCES

1. Wiplier O, Ehrenstein U. Numerical simulation of linear and nonlinear disturbance evolution in a boundary layer with compliant walls. *Journal of Fluids and Structures* 2000; **14**.
2. Davies C, Carpenter PW. Instabilities in a plane channel flow between compliant walls. *Journal of Fluid Mechanics* 1997; **352**.
3. Ehrenstein U. On the linear stabilities of channel flow over ribelets. *Physics of Fluids* 1996; **8**.
4. Luchini P. Asymptotic analysis of laminar boundary-layer flow over finely grooved surfaces. *European Journal of Mechanics B* 1995; **14**.
5. Bearman PW. Investigation of the flow behind a two-dimensional model with a blunt trailing edge with splitter plates. *Journal of Fluid Mechanics* 1965; **21**.
6. Zadravkovich MM. Review and classification of various aerodynamic and hydrodynamic means for suppressing vortex shedding. *Journal of Wind Engineering and Industrial Aerodynamics* 1981; **7**.
7. Wong HY. A means of controlling bluff body separation. *Journal of Industrial Aerodynamics* 1979; **4**.
8. Bearman PW, Harvey JK. Control of circular cylinder flow by the use of dimples. *AIAA Journal* 1993; **31**.
9. Heenan AF, Morrison JF. Passive control of pressure fluctuations generated by separated flow. *AIAA Journal* 1998; **36**.
10. Jimenez J, Uhlmann M, Pinelli A, Kawahara G. Turbulent shear flow over active and passive porous surfaces. *Journal of Fluid Mechanics* 2001; **442**.
11. Hahn S, Je J, Choi H. Direct numerical simulation of turbulent channel flow with permeable walls. *Journal of Fluid Mechanics* 2002; **450**.
12. Angot Ph, Bruneau Ch-H, Fabrie P. A penalization method to take into account obstacles in incompressible viscous flows. *Numerische Mathematik* 1999; **81**.
13. Caltagirone J-P. Sur l'interaction fluide-milieu poreux: Application au calcul des efforts exercés sur un obstacle par un fluide visqueux. *Comptes Rendus des Seances de l' Academie des Sciences* série II 1994; **318**.
14. Nield DA, Bejan A. *Convection in Porous Media*. Springer: Berlin, 1999.
15. Whitaker S. *The Method of Volume Averaging*. Kluwer: Dordrecht, 1999.
16. Beavers GD, Joseph DD. Boundary conditions at a naturally permeable wall. *Journal of Fluid Mechanics* 1967; **30**.
17. Carbou G. Asymptotic analysis for a two-scales penalization method in fluid dynamics. submitted.
18. Bruneau C-H, Fabrie P. Effective downstream boundary conditions for incompressible Navier–Stokes equations. *International Journal for Numerical Methods in Fluids* 1994; **19**.
19. Bruneau C-H, Saad M. The 2d lid-driven cavity problem revisited. submitted.
20. Bruneau C-H, Mortazavi I. Contrôle passif d'écoulements incompressibles autour d'obstacles à l'aide de milieux poreux. *Comptes Rendus des Seances de l' Academie des Sciences* série II 2001; **329**.
21. Achdou Y, Pironneau O, Valentin F. Effective boundary conditions for laminar flows over periodic rough boundaries. *Journal of Computational Physics* 1998; **147**.
22. Tabeling P. Two-dimensional turbulence: a physicist approach. *Physics Reports* 2002; **362**.
23. Kellay H, Bruneau Ch-H, Wu XL. Probability density functions of the enstrophy flux in two dimensional grid turbulence. *Physics Review Letters* 2000; **84**(8).

Copyright © 2004 John Wiley & Sons, Ltd.